Surface Topography: Metrology and Properties

Design and characterization of textured surfaces for applications in the food industry

To cite this article before publication: Gianmarco Lazzini *et al* 2017 *Surf. Topogr.: Metrol. Prop.* in press https://doi.org/10.1088/2051-672X/aa939f

Design and characterization of textured surfaces for applications in the food industry

G Lazzini[1], L Romoli[1], L Blunt[2] and L Gemini[3]

[1]Department of Engineering and Architecture, University of Parma
Parco Area delleScienze 181/A, 43124 Parma, Italy

[2]EPSRC HUB Advanced Metrology, School of Computing and Engineering,
University of Huddersfield
Queensgate, Huddersfield HD1 3DH, UK

[3]ALPhANOV, Institut d'Optique d'Aquitaine
Rue François Mitterand, 33400 Talence, France

Abstract. The aim of this work is to design,manufacture and characterize surface morphologies on AISI 316L stainless steel produced by a custom designedlaser-texturing strategy.Surface textures were characterized at a micrometric dimensionin terms of areal parameters compliant with ISO 25178 and correlations between these parameters and processing parameters (e. g. laser energy dose provided to the material, repetition rate of the laser pulses and scanning velocity) were investigated. Preliminary efforts were devoted to the research of special requirements for surface morphology that, according to the commonly accepted research on the influence of surface roughness on cellular adhesion on surfaces, should discourage the formation of biofilms. The topographical characterization of the surfaces was performed with a Coherence Scanning Interferometer. This approachshowed that increasing doses of energy provided to the surfaces increased the global level of roughness as well as the surface complexity. Moreover, the behavior of the parameters S_{pk}, S_{vk}indicates also that, due to the ablation process, an increase in the energy dose causes an averageincrease in the height of the highest peaks and in the depth of the deepest dales. The study of the density of peaks S_{pd} showed that none of the surfaces analyzed here seems to perfectly match the conditions dictated by the theories on cellular adhesion to confer antibiofouling properties. However, this result seems to be mainly due to the limits in the resolving power of Coherence Scanning Interferometry, which does not allow the resolution of sub-micrometric featureswhich could be crucial in the prevention of cellular attachment.

Nomenclature

Symbol	Name	Unity of measure
RR	Laser repetition rate	kHz
v	Scanning speed	mm/s
HOL	Horizontal overlap	dimensionless
H	Hatch distance	mm
F	Laser fluence	J/cm^2

N	Number of Scans	dimensionless
E	Energy dose	J/cm^2
S_a	Average roughness	μm
S_q	RMS roughness	μm
S_{sk}	Skewness	dimensionless
S_{dr}	Developed interfacial area ratio	dimensionless
S_{pd}	Density of peaks	μm^{-2}
S_k	Core roughness	μm
S_{pk}	Reduced peak height	μm
S_{vk}	Reduced valley depth	μm
S_z	Maximum height	μm

1.Introduction

There are several examples of surface nano and micro structures with diverse properties that exist in nature [1, 2, 3, 4]. The self-cleaning effect of lotus leaves, the adhesion of gecko's feet, the antireflectivity of moth eyes and the antiflouling properties of fish scales are well known examples of such natural phenomena. As a result of these unique surface properties, there has been growing interest in biological interfaces and their unique features and this has encouraged scientists and engineers to investigate the physico-chemical nature of such surface structures.The ultimate goal of this biomimetic surface research is the realization of synthetic surfaces reproducing the physico-chemical properties observed in living systems, that could potentially be implemented in technological applications [5]. The ability to prevent the formation of biofilm is amongst the most reproducible features of biological interfaces. Synthetic interfaces with these properties have already gained relevance in numerous technological applications. Among these, one of the most relevant is the food industry.In particular, the formation of biofilms on the surface of food machinery can compromise food hygiene, because biofilms often contain spoilage or pathogenic bacteria, that can be dangerous for human health. In addition, the presence of biofilm on surfaces acrossfood plants can seriously limit the process yield; for example, the occurrence of biofilms can increase the frequency of plant shut down for cleaning, itcan reduce heat transfer and operating efficiency in heat exchange equipment, and evenincrease frictional resistance and corrosion rates on surfaces, leading to high losses of energy and spoiling of food stuffs [6, 7, 8].

Many unique properties of bio surfaces are correlated with the presence of surface micro- and/or nanostructures [5, 9, 10]. Numerous techniques have been explored with respect to production of bio inspired large area topographies these have included, photolitography [11, 12], nanoprinting [13, 14], and electron beam lithography [15, 16] . These techniques offer the possibility to realize structures with well defined geometries repeated periodically on a workpiece surface. Consequently, such textures are completely identified by a relatively small number of simple geometrical parameters, like the size and period of the repeating unit. These regular structures are useful for studying the correlations between the macroscopic properties and the surface morphology [11]. However, despite their excellent performance, these approaches suffer from some shortcomings, such as complexity (multiple processing steps), the need for expensive masks, the high process cost and slowness of the pattering process [10]. Recently, novel powerful approaches for the realization of biomimetic interfaces have been developed that combine the effectivenessof functional surface topographies with the possibility of

76   functionalizing largeareas,making them more suitable for up-scaling to production enivonments. These

77   techniques cover anodization [17], polymer film roughneing [18, 19], electroerosion [20], and sol-gel processes

78   [21, 22]. In particular, laser machining has emerged as a novel and promising approach for high speed

79   modification of interfacial properties; in fact, this technique, especially with ultrashort laser pulses,can facilitate

80   the realization of surface textures on multiple dimensional scales, similar to those found in natural biological

81   systems, in only a one-step process [23, 24, 25]. Moreover, these textures can be realized without the need for

82   clean room facilities and can be implemented in different gaseous atmospheres with the additional possibility of

83   controllingto some degree the surface chemistry [10]. This technique leads to surface topographies characterized

84   by a random distribution of hills and dales (ISO 25178). This fact, often accompanied by inhomogeneities in the

85   chemical composition, leads to a difficult correlation between the topographic features and the macroscopic

86   properties of interest. Therefore, an accurate description of the geometry of such random topographies requires

87   the use of statistical quantities related to the distribution of the surface topgraphical features of the processed

88   area. The need for a complete descritption of surface roughness led to the development of areal surface

89   roughness parametersand their adoption into standards (ISO 25178) [26, 27]. Unfortunately, despite this new

90   approach to surface characterisation, the majority of literature concerning the metrological characterization of

91   biomimetic interfaces restrict analysis to a few metrological quantities, such as the so-called average roughness

92   (S_a) or the RMS roughness (S_q). This kind of description is not sufficient for a complete geometrical

93   characterization of the topography, since it is known that surfaces with the same values of these parameters can

94   have different geometriesin terms of spatial properties and spatial frequency and this consequently has a great

95   affect on the surface functional properties [28, 29]. Therefore, efforts need to be devoted to introduce the use of

96   more representative parameters form the ISO 25178 "toolbox"to give a more refined description of complex

97   textures.

98   In this work, the surface roughness of AISI316L stainless steel samples treated with ultrashort laser pulseshas

99   been characterized in order to provide examples of surfaces that can be investigated for their antibiofouling

100   properties. AISI 316L austenitic stainless steel is widely used in the food industry because of its high resistance

101   to corrosion by food products and detergents [30]. Several attempts have been made to correlate the occurrence

102   of biofilm to the surface roughness of such stainless steel. Despite in this workinto the relationship between the

103   level of hygiene and the type of finishing, the published results are somehow contradictory [30, 31]. For example

104   many studies attribute the improved hygienic properties of certain finishes to the low average roughness R_a [32,

105   33] , while in other studies no clear relationships has been found between the amount of biofilm and average

106   roughness R_a [34].

107   The present studyextends the use of areal surface parameters,metrological surface parameters to include those

108   falling within the scope of standardISO 25178. The parameters have been deployed in the reported workin order

109   to assess the correlation between surface roughness and processing conditions, i. e. laser energy dose provided to

110   the target. The list of roughness parameters includes: average roughness S_a, RMS roughness S_q, skewness S_{sk},

111   developed interfacial area ratio S_{dr}, density of peaks S_{pd}, core roughness S_k, reduced valley depth S_{vk} and reduced

112   peak height S_{pk}. The metrological analysis has been performed from topographical maps obtained using a

113   Coherence Scanning Interferometer, measuring at or just below micrometric resolution. The present reported

114   work assessing optimal requirements for the antibiofouling has been carried within the framework of the basic

115   theories concerning the influence of surface roughness on bacterial adhesion.Finally, guidelines for the design of

116   surfaces minimazing the nesting of microorganisms of stainless steel surfaces, are derived and reported.

117

2.Requirements for the design of antibiofouling surfaces

119

120   With regard to the relation between surface roughness and the formation of biofilm, several theories and

121   mechanisms of adhesion have been proposed. First of all, a cell can be characterized as anexternal wall with a

122   certain degree of elasticity. Several works in literature show that the elastic modulus and non-covalent

123   interactions between a surface and the cell contribute decisively to the adhesive strength [35, 36, 37]. In the

124   formation of a biofilm, the cell wall can change its shape up to a certain limit in order to adapt itself to the

125   substrate geometry. Therefore, cells tend to adhere preferentially to surfaces that minimize the deformation of the

126   cell itself, such assurfaces with favourably sizedvalleys or grooves. These surface features are supposed also to

127   protect the cell against hydrodynamic turbulences [29, 35, 36, 37]. For example, Verran et al. showed that in

128   samples with a substrate of PMMA with an average roughness of 1.96 μm, *Candida Albicans* adhere

129   preferentially into defects, i.e. scratches [37]. Whitehead et al. observed the same behaviour for *S. aureus* and *P.*

130   *Aeruginosa*on Si surfaces coated with Ti, characterized by pits with diameter ranging from "*fractions of μm to 2*

131   *μm*" [38].

132   In the attempt to adapt the cell curvature to a surface, the base cellular shape could play a crucial role. In

133   particular, one can expect that cells, such as coccoid bacteria, with an almost spherically symmetrical shape,

134   could adapt their surface curvature to a larger variety of rough patterns than cells, such as *Pseudomonas* bacteria,

135   that have a rod-like shape, i.e. an almost cylindrical symmetry. Cellular adhesion on surfaces is in principle

136   influenced not only by the geometrical characteristic of cells, but also by other factors, like the ability to secrete

137   polymeric substances that facilitate the attachment and experimental results that have been published over the

138   years seem to confirm this hypothesis. For example, Ivanova et al. showed that the spherical *S. aureus* cells

139   adhere more easily on molecularly smooth Ti surfaces compared to the rod-like *P. aeruginosa* [39]. They

140   attribute this effect not only to the shape of bacteria, but also to the more flexible cell membrane in *S. aureus*

141   than in *P. aeruginosa*. For this last reason *S. aureus* can adhere easily on a surface with spikes whose spacing

142   dimension are lower than cellular size, by adapting its outer structure to the surface curvature. In these and other

143   examples [23, 39, 40, 41], the emerging common concept is that the bacterial dimension defines a critical length-

144   scale for bacterial adhesion: structures whose size is smaller than the cellular dimension have negligible effect on

145   bacterial attachment. This idea explains some conventions that have been introduced in the design of surfaces

146   utilised in the food industry, for example the rule that hygenic steel surfaces must have an average roughness

147   lower than 0.8 μm dictated by the EHEDG (European Hygienic Equipment Design Group) and additionallythe

148   requirement of R_a less than 1.6 μm, dictated by the ISO 4287 standard for cleanability,[31, 37] The idea of a

149   "cutoff" threshold length scale of 0.2 μm for the formation of bacterial plaque on dental surface is proposed by

150   Bollen et al [42]. To clarify this point, the authors report the argument proposed by Scardino et al. [43], who

151   studied the attachment of diatom cells of different sizes on polymide surfaces with grooves modelled from the

152 fouling resistant bivalves *Mytilus galloprovincialis* and *Tellina plicata*. They found that for groove widths near

153 the cells size, the number of adhered cells decreases significantly. The schematic diagram used to explain this

154 behaviour is reported in figure 1. A cell standing on a surface whose roughness is larger than the cell size (fig.

155 1(a)) adheres on the surface with a relatively large number of attachment points. On the contrary, a surface

156 whose roughness is smaller than the cell size provides a small number of attachment points, thus making more

157 difficult the cellular adhesion (fig. 1 (b)).

158

159
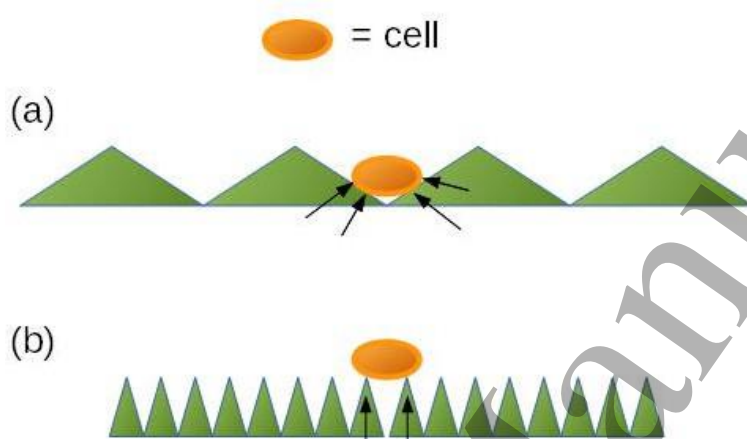
160

161

162

163 Figure 1. Scheme proposed to explain the correlation between diatom cell size and width of grooves in a rough

164 surface.

165

166 According to the hypotheses defined so far and taking into account that the average surface roughness S_a

167 obtained by conventional machining ranges between 3.2 to 1 μm, the most frequent condition when generating

168 surface texture by mechanical tools would be that represented in panel a of figure 1: the alternation of peaks and

169 valleys would create a favourable condition to host microorganisms. Therefore, the main idea is to look for a

170 technological process which enables the production of multiscale hierarchical structures in which nanoscale

171 features are superimposed to the microscale roughness. With these surface morphologies, the condition that

172 minimizes the number of contact points depicted in the panel b of figure 1 should be present across the surface

173 including the inclined flanks of the primary roughness. It should be noted that defining optimal attachment

174 criteria by S_a values alone is essentailly flawed as S_a refers only to surface amplitude information and does not

175 infer spatial properties. In fact two surface of differeing roughness (S_a) could have identical spatial properties. A

176 better quantifying parameter should be a roughness parameter based on spatial information such as peak density

177 S_{pd} combined with a parameter inferring amplitude properties.

178

179 In order to define the number of peaks per area unit that an ideal surface should have to hinder the multiplication

180 of contact point between bacteria and surface, the attachment behaviour of *S. aureus,*which is represented as a

181 blue circle in figure 2, was investigated. A single cell of this bacterium has an approximately spherical shape,

182   whose diameter d is in the range 0.5-0.7μm. Hence a critical value of density of peaks S_{pd} can be defined which

183   corresponds to a distance between adjacent peaks equal to the cellular diameter. This value is such that $(1/S_{pd})^{1/2} \approx$

184   d , and it is equal to $S_{pd}^{crit} \approx 4\ \mu$m^{-2}. For S_{pd} such that $S_{pd} < S_{pd}^{crit}$, we can expect that the most part of bacterial cells

185   will stand on the bottom of valleys, thus maximizing the contact area. In addition, since the reduced valley depth

186   S_{vk} (see appendix for the formal definition) is related to the surface depth in the bottom of the dales, one can

187   expect a correlation between the amount of biofilm and S_{vk}. For high S_{pd}, i. e. such that $S_{pd} > S_{pd}^{crit}$, the bacteria

188   will remain in contact with the peaks. Therefore, in an attempt to prevent the formation of biofilm, this situation

189   has to be considered preferable. By the definition the reduced peak height parameter S_{pk}, should be correlated

190   with the surface height above the mean plane. Therefore, for $S_{pd} > S_{pd}^{crit}$, we can expect a strong correlation

191   between this parameter and the amount of biofilm. Finally, for intermediate values of peak density, S_{pd} it can be

192   expected that a significant part of the cell surfaces will stand in contact with the sample surface at intermediate

193   heights with respect to the mean height line. Consequently, it can be surmised that there should be a correlation

194   between the amount of biofilm and the core roughness S_k, that, according to its definition, is related to the core

195   height of the surface. However, it is important to emphasize that at the moment these arguments are only

196   hypothetical and do not account for additional effects, such as disomogeneities in the chemical composition from

197   the summit to the valleys, bacterial motility, dynamics of the fluid containing the bacteria etc. Therefore, these

198   theories need to be investigated experimentally.

199
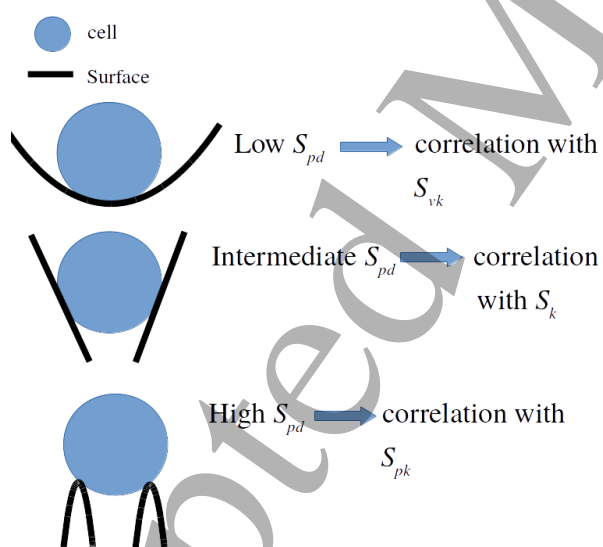
200
201 Figure 2. Schematic illustration of the possible correlations between the amount of bacterial adhesion and the
202 parameters S_{vk}, S_{pk} and S_k in relation with the value of S_{pd}.

203

204 **3. Materials and laser processing**

205

206   In order to assess the optimal surface topographies for antifouling a series of irradiated samples consisting of

207   square plates of 50 mm side and thickness of 2 mm, made of AISI 316L stainless steel were examined. AISI

208   316L was chosen as the target material as it is widely employed in food handling and food processing. All the

209   samples had a baseline as-received average roughness $S_a < 0.5\ \mu$m. Before the laser treatment, the samples were

210   cleaned for 5 minutes in acetone in an ultrasound bath, following this laser texturing was performed without

211 shielding gas. Textured surfaces with dimensions of 8×8 mm^2 were obtained by irradiation with linearly

212 horizontally polarized pulses of an Amplitude Systems Satsuma HP3 laser system with average power up to 40

213 W, the repetition ranged up to 1 MHz, the central wavelength was 1030 nm and the pulse duration was 350 fs.

214 The laser beam was firstly magnified by a factor of three through a beam expander and then directed into a

215 scanning system to provide accurate positioning of the laser pulses. The final focus was achieved using a 100

216 mm f-theta lens to a spot diameter of approximately 25 μm. The laser pulse repetition rate,RR and scan speed

217 the scan speedare indicated below.Four different experimental conditions were examined: RR=100 kHz and v =

218 200 mm/s, RR=250 kHz and v = 500 mm/s, RR=500 kHz and v = 1000 mm/s, and finally RR=1000 kHz and v =

219 2000 mm/s. The horizontal overlap $HOL$is defined as :

220

221 $$HOL = \frac{d-l}{d} \times 100 \qquad\qquad (1)$$

222

223 where d is the beam diameter and l is the length of the path made by the laser source between two consecutive

224 pulses ($l = v/RR$). The processing conditions specified above were set to maintain the horizontal overlap at 92%,

225 in order to maximize the efficiency of laser ablation. For each combination of scan speed and repetition rate, nine

226 values of laser fluence F(defined as the ratio between the pulse energy and the focused spot area) were chosen,

227 ranging from 0.36 to 2.33J/cm^2. The selected range of F was established based on a lower limit necessary to

228 overcome the specific modification threshold of the material and an upper limit to avoid thermal damage and

229 surface melting. A factorial design of experiments was then developed with 4 levels of repetition rate and 9

230 levels of fluence, giving a total of 36 textured surfaces.

231 The energy dose,E,was defined as the ratio between the total energy provided to the surface by the radiation and

232 the total irradiated area. Higher energy dose regimes could potentially be achieved also by superimposing

233 multiple successive scans, N. In particular, for this experiment, the same process was repeated for N = 10 scans.

234 Therefore, by neglecting thermal losses between two consecutive scans, the total energy doses provided to the

235 surfaces ranged from 178 to 1143J/cm^2. Prior to surface characterization, the treated surfaces were emersed in an

236 ultrasonic bath for 10 minutes using ethanol at room temperature, they were then washed with fresh ethanol and

237 finally dried in vacuum at room temperature.

238 For sake of clarity Table 1 summarizes the process parameters used for the tests together with other process

239 variables which were kept constant in the present study.

240 Table 1. Process parameters and range of variation. Scan speed was varied according to repetition rate to keep
241   the overlap constant at 92%.

	Value/Range
Wavelength	1030 nm
Pulse duration	350 fs
Repetition rate, RR	100, 250, 500, 1000 kHz
Spot diameter	25 µm
Pulse overlap, HOL	92%

Scan speed, v	200, 500, 1000, 2000 mm/s
Hatch distance, H	5 µm
Laser fluence, F	0.36, 0.48, 0.69, 0.86, 1.14, 1.35, 1.69, 1.94, 2.33 J/cm^2
Number of scans, N	10
Energy dose, E	178, 235, 340, 423, 560, 663, 831, 950, 1143 J/cm^2

4. Surface characterization

Surfaces have been firstly inspected from a qualitative point of view using a Phenom desktop scanning electron microscope (SEM). This was done with the objective to ascertain the presence of hierarchical structures by using the maximum allowed depth of focus of the scanning electron microscope at a magnification up to 6000x. The topography of the surfaces as quantified using a Coherence Scanning Interferometer. The experimental apparatus employed was the Taylor-Hobson CCI MP. A 50x objective was used with a Numerical aperture of 0.55 and working distance of 3.4mm. The maximum measurement area is square of size $336 \times 336 \ \mu m^2$ where the optical lateral resolving power of the objective is limited to $0.4 \mu m$ the acquisition software can produce digital maps whose maximum size is 1024×1024 resulting from interpolation procedures. Therefore, the effective resolving power can reach nominal values of approximately 338 nm. A problem concerning the data acquisition with Coherence Scanning Interferometry is related to the fact that, with the numerical aperture specified, the apparatus cannot detect signals originating from surfaces whose slopes are greater than 27.5deg. This limit is due to the fact that the light is scattered from the slopes away from the acceptance cone of the objective. This drawback results in the presence of non measured points in the digital maps. To limit this problem, a data binning protocol was applied to the acquired matrices, reducing the size of the maps to 512×512. This level of binning is a reasonable compromise between the need to minimize the number of non-measured points and the need to minimize the number of optical artifacts in the form of non-physical peaks..

The interferometric maps were first subjected to a spline interpolation procedure, whose aim was to "fill in" the non-measured points resulting from the finite acceptance angle of the objective. The calculation of metrological parameters was performed on previously filtered digital maps. The filtering procedure included a least squares leveling operation, and a Gaussian S-filter with a cutoff wavelength of $2.1 \mu m$ on both the x and y directions. This filtering procedure had the purpose of cutting-off the noise observed mainly in the maps obtained with low energy doses. The procedures followed for the calculation of the roughness parameters described in this work are expleined in detail in the appendix.

5. Results and discussion

In figure 3 a series of SEM images of portions of surfaces obtained with different values of RR and v and for growing values of E provided to the samples is reported. At low E, laser-induced periodic surfaces structures (LIPSS) called LSFL (Low Spatial Frequency LIPSS) are observed. These structures are oriented

275 perpendicularly to the laser polarization and with a period comparable to the laser wavelength. The presence of

276 LSFL in similar conditions of irradiation has been previously assessed in other works in literature [44, 45, 46,

277 47].

278
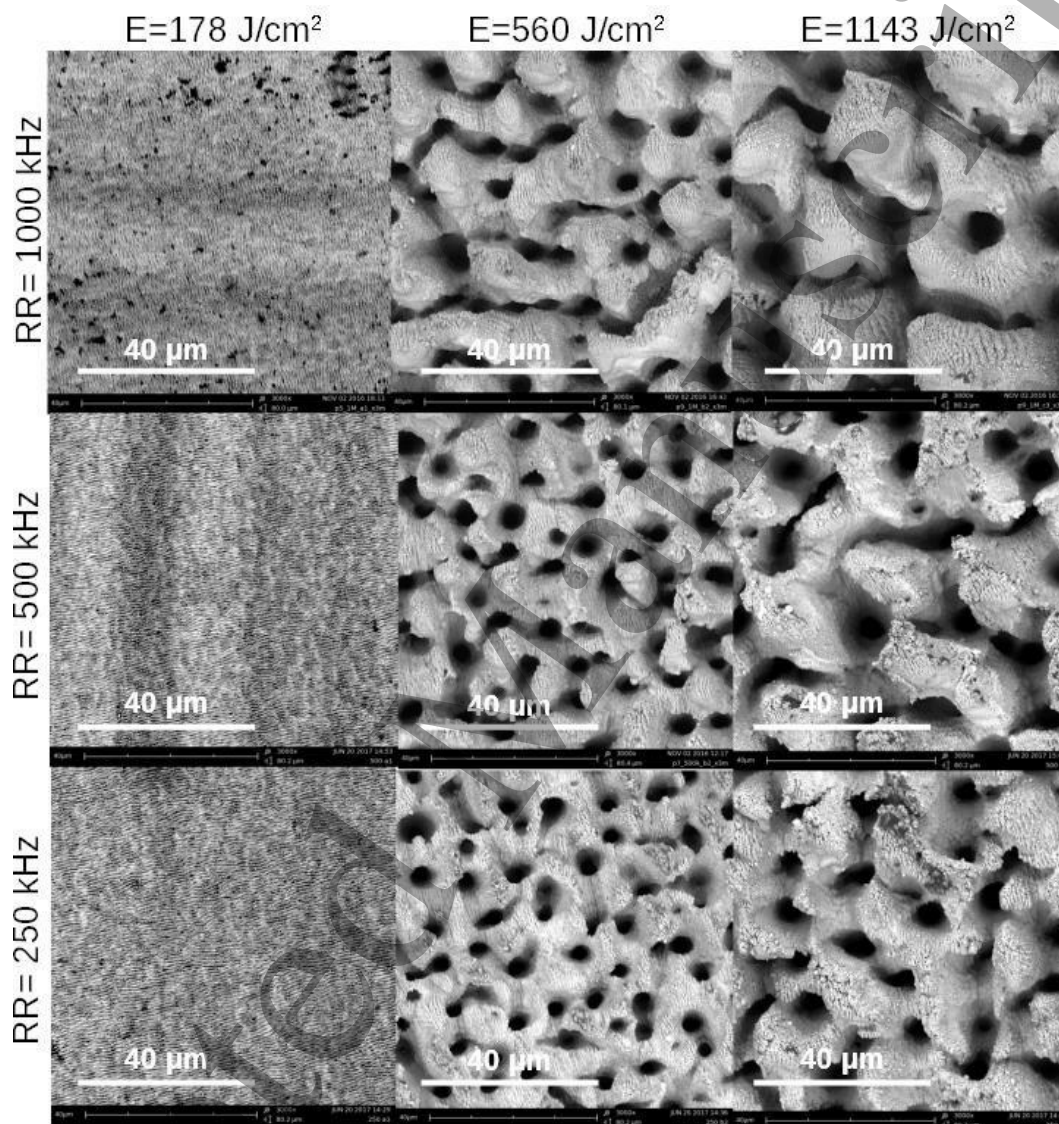
280 Figure 3. SEM images of the laser ablated surfaces obtained with different values of *RR*(on the left) and for

281 growing values of *E* (on the top) provided to the samples.

282

283 By increasing the *E* parameter, LIPSS are replacedwith columnar structures whose transversal dimensions

284 increase with increasing *E*. In addition, it's possible to distinguish periodic features, situated on the top of such

285 columnar structures. SEM images obtained at higher resolutions than those showed in fig. 3 reveal that these

286 periodic features have a period comparable with the laser wavelength. Another interesting feature concerning the

287 experimental conditions with which the laser texturing has been performed is the variation of the surface

288 morphology with the *RR* for a given value of energy dose *E*. In particular, by fixing *E*, a decrease in *RR* seems to

289 reduce the transversal dimension of the columnar structures.

290   Several physical phenomena are expected to contribute to the morphologies observed. First of all, at lower

291   energy doses Marangoni convection, driven by the high thermal gradients generated by the ultrafast laser-matter

292   interaction, has been proposed as the dominant physical process that occurrs [48]. At higher E, the common idea

293   is that the surface morphology is the result of a modulated energy deposition due to the interference between the

294   laser pulses and surface plasmon polaritons (SPP). By further increasing the E parameter, the carrier densities

295   reach values for which the formation of SPPs can't occurr anymore. In this situation, the dominant mechanisms

296   that control the surface morphology change and a transition from LIPSS to bumps is observed.

297   The decrease in the spike width for decreasing values of RR is confirmed by a qualitative analysis of the

298   interferometric maps reported in figure 4. In fact, in the topographic view we observe a decrease in the height of

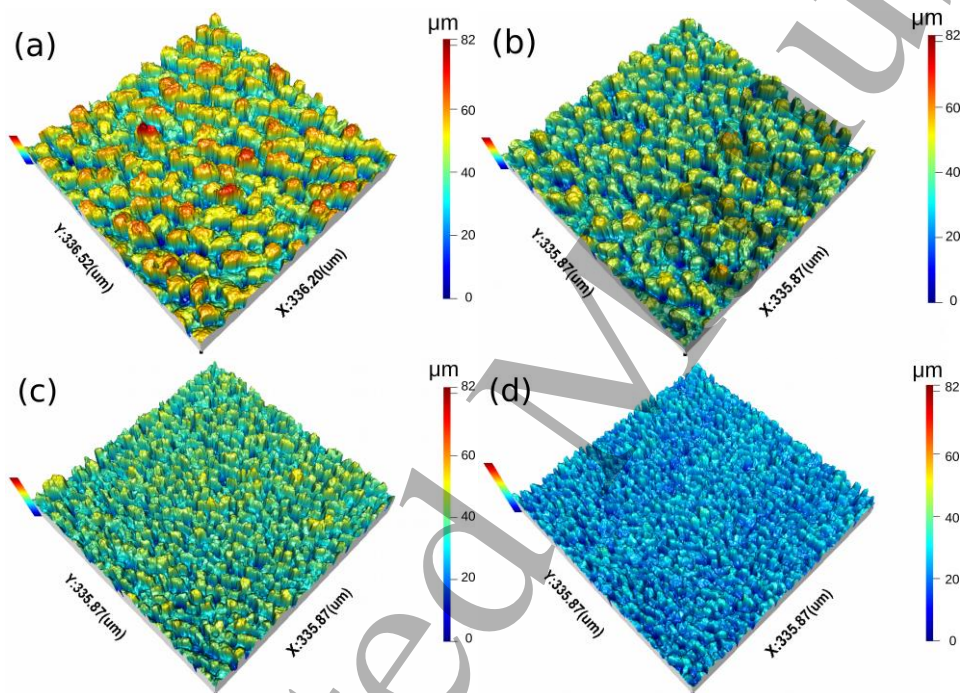299   the structures by decreasing the repetition rate

300
301

302

303
304
305

306   Figure 4. Interferometric 3D maps regarding textures obtained using E=1143J/cm^2: (a) RR=1000 kHz, v =
307   2000mm/s; (b) RR= 500 kHz, v = 1000mm/s; (c) RR=250 kHz, v = 500mm/s; (d) RR=100 kHz, v= 200mm/s.

308
309   In figs. 5 and 6 the plot of the average roughness S_a and RMS roughness S_q vs the energy dose E is shown. The

310   two graphs show that S_a and S_q increase almost linearly with E, indicating that the increase in the transversal size

311   with E showed in figure 3 is accompanied by an increase in the average height. The slope of the linear

312   dependence decreases for decreasing values of repetition rate.

313
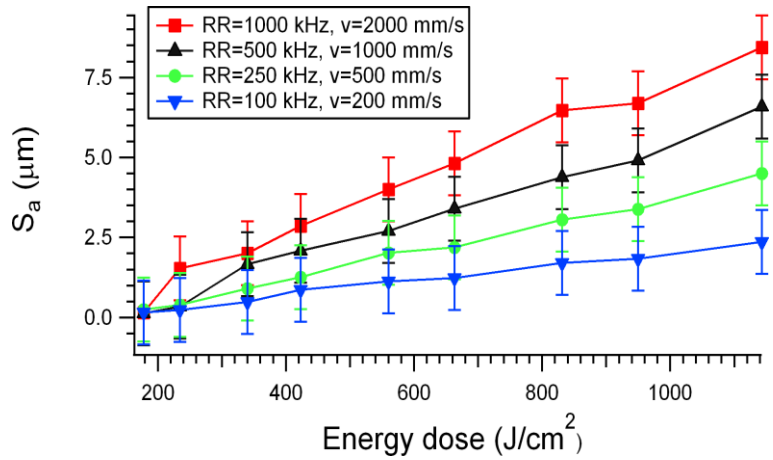
314
315   Figure   5.Evolution of the average roughness S_a with the energy dose $E$for ultrashort laser textured surfaces
316   (evaluation area: $336 \times 336 \ \mu m^2$). The error bars associated to the values of E have the same size of the markers
317   (standard deviation).

318
319
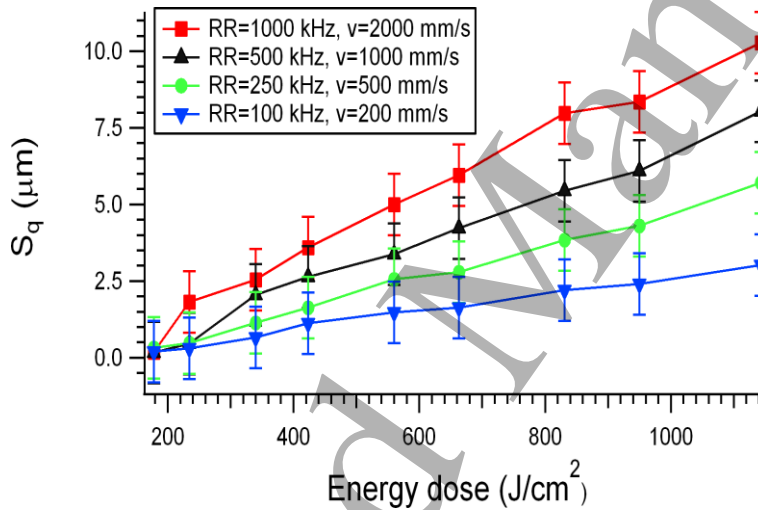
320
321   Figure   6.Evolution of the RMS roughness S_q with the energy dose $E$for ultrashort laser textured surfaces
322   (evaluation area: $336 \times 336 \ \mu m^2$). The error bars associated to the values of E have the same size of the markers
323   (standard deviation).

324
325   While the correlation expressed in figs 5-6 are quite well defined, the correlation between E and the skewness S_{sk}

326   (figure7) is less evident. However, some interesting conclusions can be drawn by observing this last parameter.

327   S_{sk} seems to be almost constant or weakly decreasing as a function of E for all the experimental conditions..

328   According to the definition of S_{sk} [49], the decrease of S_{sk} for decreasing values of RR means that the surface is

329   increasing valley dominated. This increasingly negative value will be self limiting and then reverse when the so

330   called valleys grow in lateral extent to a point where the calculated mean plane shifts downwards. This effect is

331   due to the ablation of material that, according to the qualitative observations made on the interferometric maps, is

332   more effective   for low values of RR and v where the valley features are relatively isolated compared to the
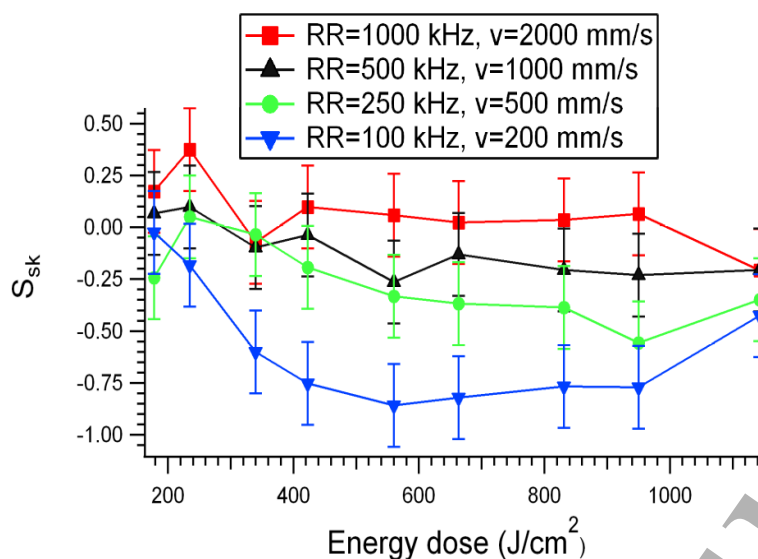
333   surrounding topography[50].

334

335
336 Figure 7.Evolution of the skewnessS_{sk} with the energy dose E for ultrashort laser textured surfaces (evaluation
337 area: 336 ×336 μm^2). The error bars associated to the values of E have the same size of the markers (standard
338 deviation).
339

340 With regard to the behaviour of S_{dr}, a strong correlation between this parameter and E was observed. In particular

341 an increasing level with E similar to that found for S_a and S_q was observed. The S_{dr} parameter takes account of

342 the ratio between the actual surface area and the projected measurment area (for further information, see the

343 appendix). Therefore, it can be seen that the ablation process increases the total interfacial area with energy

344 doses. According to some studies on the influence of surface roughness on bacterial adhesion [24], an increase in

345 the interfacial area is not necessairly reflected in an increase in the surface available for cellular attachment.In

346 particular, as we pointed out in the section 2, large areas could trap air bubbles, thus hindering cellular adhesion.

347 Further investigations on the bacterial attachment have to be performed in order to clarify this point.
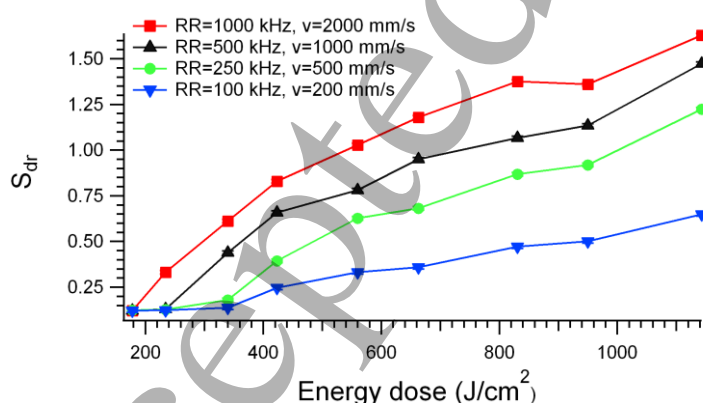
348

349
350 Figure 8.Evolution of the developed area ratio S_{dr} with the energy dose E for ultrashort laser textured surfaces
351 (evaluation area: 336 ×336 μm^2). The error bars associated to the values of E and S_{dr} have the same size of the
352 markers (standard deviation).
353

354
355

356

357 In figure9 the density of peaks S_{pd} is plotted versus the quantity E. First of all, we note that the reported curves,

358 corresponding to fixed values of RR, have a well defined behaviour for high energy doses, in accordance with the

359 qualitative observation of SEM and interferometric data. In particular, for fixed RR, S_{pd} decreases with increasing

360 E, with a rate depending on the repetition rate, indicating an increase in the overall size of the surface structures.

361 In addition, a decrease in RR at fixed E leads to textures with denserpeaks, with greater values of S_{pd}. This trend

362 confirms the qualitative observations made on the interferometric maps. For decreasing energy doses, the limits

363 in the resolution of the Coherence Scanning Interferometer become more and more evident. In particular, the

364 calculation of S_{pd} is heavily affected by the occurrence of the transition between bumps and LIPSS, represented

365 approximately by the dashed vertical line in figure 9. Another crucial point is that none of the surfaces examined

366 here seem to match the condition on the values of S_{pd} defined in section 2. However, peaks of sizes of 1 - 1.5 μm

367 are distinguishable in the SEM images (figure 3, for $E = 178.0$ J/cm^2). Such peaks either cannot be resolved in

368 the interferometric maps, or they are excluded from the counting of peaks by the procedure for the calculation of

369 S_{pd} dictated by the ISO standard. Moreover, SEM images obtained with higher resolution show that all the

370 surfaces present a hierarchical shape. Therefore, an additional investigations on the S_{pd} parameter with

371 microscopies that allow to resolve sub-micrometric features and concrete tests on the bacterial adhesion are

372 needed in order to clarify this point. In addition we cannot exclude effects of the extracellular polymeric

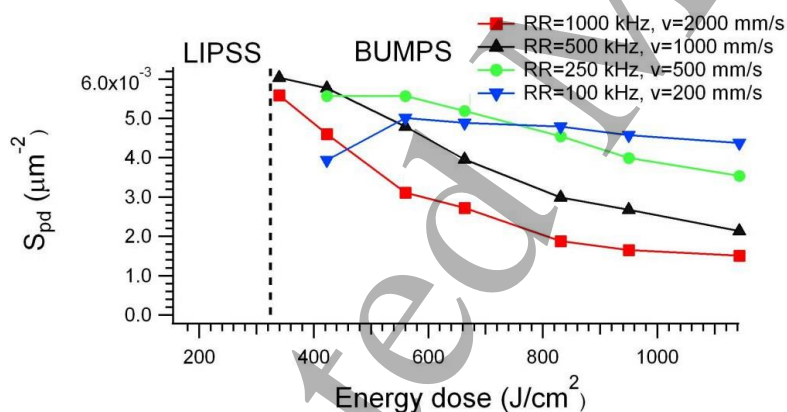373 substance or of the cell curvature that should in principle relax the requirements made here.

374

375
376
377 Figure 9.Evolution of the density of peaks S_{pd} with the energy dose $E$for ultrashort laser textured surfaces
378 (evaluation area: 336 $\times$336 μm^2). The dashed vertical line represents a a qualitative estimate of the value of E at
379 which a transition between bumps and LIPSS occurrs. The error bars associated to the values of E have the same
380 size of the markers (standard deviation).

381

382 In figures10-12 the parameters S_k, S_{pk} and S_{vk} as a function of $E$are shown. All the parameters show an increasing

383 behaviour for increasing values of $E$with a growth rate that decreases for decreases in RR. This behaviour is more

384 evident on the S_k parameter, that is related to the depth of the core roughness. The behaviour of S_k has similarities

385 to that of S_a and $S_a$since S_k measures an amplitude property.

386
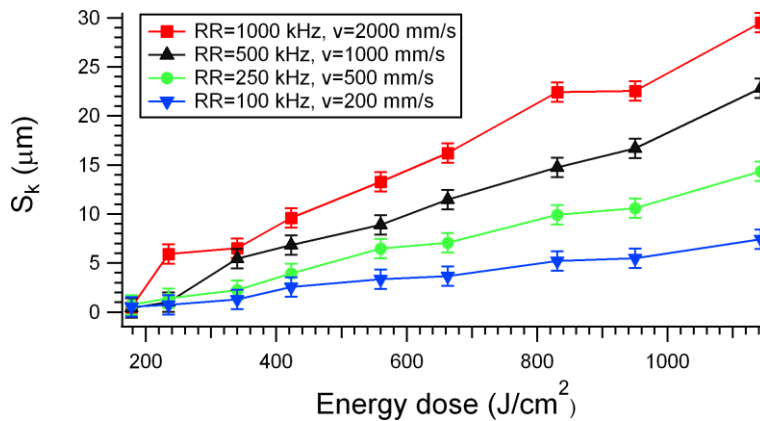
387
388 Figure 10.Evolution of the core roughness S_k with the energy dose E for ultrashort laser textured surfaces
389 (evaluation area: $336 \times 336 \ \mu m^2$). The error bars associated to the values of E have the same size of the markers
390 (standard deviation).

391
392
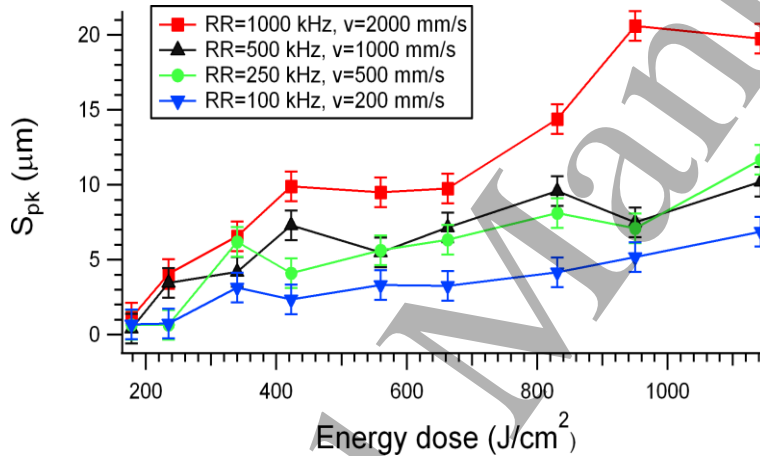
393
394 Figure 11.Evolution of the reduced peak height S_{pk} with the energy dose E for ultrashort laser textured surfaces
395 (evaluation area: $336 \times 336 \ \mu m^2$). The error bars associated to the values of E have the same size of the markers
396 (standard deviation).

397
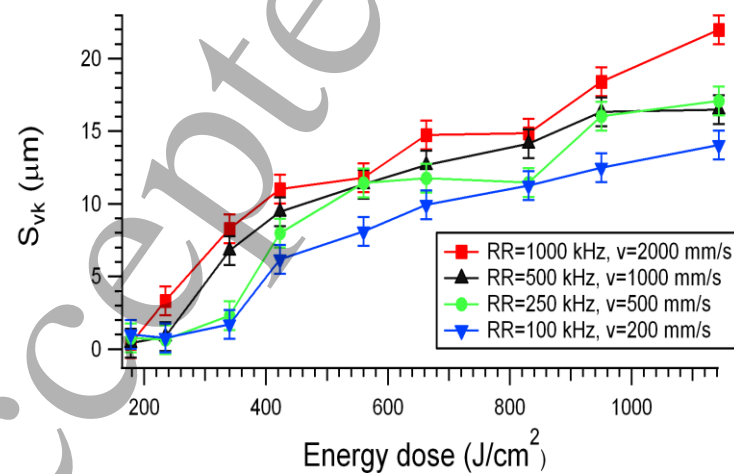
398
399 Figure 12.Evolution of the reduced valley depth S_{vk} with the energy dose E for ultrashort laser textured surfaces
400 (evaluation area: $336 \times 336 \ \mu m^2$). The error bars associated to the values of E have the same size of the markers.

401

402 According to the definitions of S_{pk} and S_{vk}, the graphs observed in figs. 11 and 12 show that the increase in E
403 causes an increase in the depth of the highest peaks (S_{pk} vs E) and an increase in the depth of the deepest dales
404 (S_{vk} vs E). However, S_{pk} seems to be more sensitive to the choice of RR than S_{vk}.

405

406 ## 6. Further development

407

408 According to the main theories on the correlation between surface roughness and cellular adhesion, outlined in
409 the section 2, the laser treatments regarding the surfaces obtained at energy doses greater than 235 J/cm^2 seem to
410 be not suitable for the realization of antibacterial surfaces, i. e. do not satisfy the condition outlined in the section
411 2 for antibacterial surfaces. Unfortunately, the resolution of the Coherence Scanning Interferometer employed to
412 perform the topographical analysis of the surfaces didn't allow full resolution of the surface structures obtained
413 at energy doses less than 235 J/cm^2. Further investigations are needed in order to obtain topographical maps with
414 better resolution. Furthermore, concrete measurements of bacterial attachment have to be performed in order to
415 assess if these surfaces are antibacterial with respect to the non treated substrate and to quantify whether the
416 amount of biofilm is correlated with the specific processing conditions. In addition, it could be interesting verify
417 which parts of the surface texture bacterial cells adhere preferentially, in order to establish if the conditions
418 defined in the section 2, based on the so-called "sheltering effect" and on the contact area between a single cell
419 and the substratum are correct. However, the general conclusion that can be drawn from the overall
420 topographical analysis is that structures with smaller and denser surface structures have to be realized in order to
421 reach the size of bacterial cells. This aim could be reached with two strategies. First of all, one of the advantages
422 provided by ultrashort laser treatment is the possibility to obtain hierarchical surface structures with a relatively
423 low number of pulses. Therefore, for laser fluences well above the ablation threshold, a reduction in the number
424 of passes provided to the target could reduce the risk to partially cancel the structures created by the first pulses.
425 Secondly, according to the main theories on the formation of LIPSS [25], smaller structures could be obtained
426 with lower wavelengths, e. g. by working in the UV spectrum. Another open point is the influence of the surface
427 chemistry induced by the laser processing on the bacterial attachment. The leser treatment induces the formation
428 of a layer of oxide [51]. However, it isn't clear how the interaction between this layer and the cell wall or the
429 extracellular polymeric substance influences bacterial adhesion. Therefore, further investigations on chemical
430 nature of the surfaces realized, e. g. XPS spectrometry, could be useful to clarify this point.

431

432

433

434 ## 7.Conclusions

435

436 In this work a detailed characterization of surface morphology of stainless steel surfaces textured by an ultrashort
437 pulsed laser was performed. The metrological parameters employed have been calculated within the framework
438 of the standard ISO 25178. It is evident however that the laser ablation increases the global level of roughness as
439 a functions of the energy dose E. This trend means that there is an increase in the average height of surface

440   structures, evident in the behaviour of S_a and S_q, an increase in the average peak spacing, as shown in the

441   behaviour of S_{pd}, and and increase in the core height, as shown by S_k, when the energy dose delivered to the

442   surface increases. The calculation performed indicate also S_{sk} is less easy to control by acting on the laser

443   parameters. However, the substantial behaviour of such parameter indicates that the laser ablation increases the

444   fraction of surface occupied by dales over the fraction occupied by peaks. The S_{dr} parameter reveales that, for

445   growing energy doses, the total surface area increases, due to the ablation process. As pointed out in the section

446   5, we cannot as yet establish if this property is deleterious in the attempt to realize an antibiofouling surface. In

447   particular further investigations on the power of trapping air bubbles and experiments on bacterial adhesion are

448   needed in order to clarify this points. Finally, the parameters S_{pk} and S_{vk} show that the increase in the structure

449   size corresponds to a relative decrease in the average heights of peaks and dales. In addition it was ascertained

450   that none of the surfaces examined seems to match the conditions on S_{pd} defined to grant an antibiofouling

451   property, at least from the measurement defined so far. Furthermore, the values of S_a observed in almost all the

452   surfaces analyzed are far greater than the thresholds of normally indicated in the commonly adopted ISO norms

453   for hygenic surfaces specified in the section 2. However, it is expected that sub-micrometric features

454   characterizing surface textures realized with ultrashort laser treatment, should lead to higher

455   values S_{pd} approaching the requested value of 4 peaks per squared micron. Analyses of biofilm formation will be

456   performed on larger areas textured with the parameters combinations hypothesized in this work in order to

457   clarify if the guidelines for the surface design are enough for a preliminary planning of anti-adhesion

458   functionalities for healthcare applications.

459
460

461   **Appendix: definitions of areal surface parameters**

462

463   In the following, metrological parameters that have been employed to decribe the topography of the surfaces

464   characterized in this article will be described. As already mentioned, all the parameter are included in the

465   standard ISO 25178. The correlation with the amount of cellular adhesion has already been observed for some of

466   the parameters presented here [52, 53, 54, 55], while for the others this correlation has to be verified with

467   experimental observations.

468   The topographical information consists in a real matrix, whose elements $\{z_{i,j}\}$, with $i=1,...,N_x$, $j=1,...,N_y$,

469   represent the local height with respect to the average plane.

470   The most commonly adopted parameter to characterize the global level of roughness is the so-called *average*

471   *roughness S_a*, defined as

472

473    $$S_a = \frac{1}{N_x N_y} \sum_{i=1}^{N_x} \sum_{j=1}^{N_y} |z_{i,j}|$$ (2)

474

475   Another widespread roughness parameter is the *RMS roughness S_q*, defined as

476

477
$$S_q = \sqrt{\frac{1}{N_x N_y} \sum_{i=1}^{N_x} \sum_{j=1}^{N_y} z_{i,j}^2}$$
(3)

478

479 Despite both S_a and S_q give a measure of the average deviation of the surface topography from the mean line

480 from the mean plane, the RMS roughness is considered more meaningful than the average roughness, because it

481 represents the standard deviation of the distribution of heights.

482 It's common for two surfaces with clearly different structures to have similar values of S_a and S_q [56].

483 Therefore, the description of surface topography is usually enriched by introducing moments of the height

484 distribution of successive orders, in particular Skewness S_{sk} and Kurtosis S_{ku} [57]. However, in this work S_{ku} has

485 been found weakly corrrelated with the processing parameters. For this reason, in this, analysis, S_{ku} has been

486 neglected.

487 The *skewness* parameter is defined as the moment of the 3rd order of the distribution of heights, and it is given

488 by

489

490
$$S_{sk} = \frac{1}{S_q^3 N_x N_y} \sum_{i=1}^{N_x} \sum_{j=1}^{N_y} z_{i,j}^3$$
(4)

491

492 Skewness quantifies the asimmetry of the distribution of heights with respect to the mean value. In particular,

493 $S_{sk} > 0$ indicates a dominance in peaks over valleys, while $S_{sk} < 0$ indicates a dominance in valleys over peaks.

494 One of the most relvant effects of laser treatment is the increase of the total interfacial area. To quantify this

495 increase, the *developed area ratio* S_{dr} has been introcuced. It is defined as

496

497
$$S_{dr} = \frac{A_{interf} - A}{A}$$
(5)

498

499 where A_{interf} is the total interface area, calculated with a process of triangulation, while A is the projection of

500 A_{interf} on the mean plane. In other words, this dimensionless parameter increases with increases of the interfacial

501 area.

502 The *density of peaks* S_{pd} is the number of peaks for unit of surface. One of the most relevant problems regarding

503 the calculation of such parameter is the tendency to overestimate the number of hills and, therefore, the value of

504 S_{pd}. According to the ISO standard employed, the S_{pd} parameter was calculated on the filtered maps by applying,

505 in sequence, the watershed algorithm on the topographical map multiplied by -1, in order to segment the hills,

506 and a Wolf pruning algorithm of 0.2 μm, in order to exclude non significant peaks from the density

507 calculations[58]. In particular, duedue the limits in the resolution specified in the section 5, the surface analysis

508 was limited to the micrometric motifs. All the calculations were preformed on an evaluation area of 336×336

509 μm^2. This area was judged large enough to ensure a stathistical significance to the calculations.

510 Finally, the so-called functional parameters, the *core roughness* S_k, the *reduced peak height* S_{pk} and the *reduced*

511 *valley depth* S_{vk} have been analyzed. These parameters are derived from the so called *Abbott-Firestone curve*,

512 defined as the integral of the distribution of heights (see fig. 1).

513
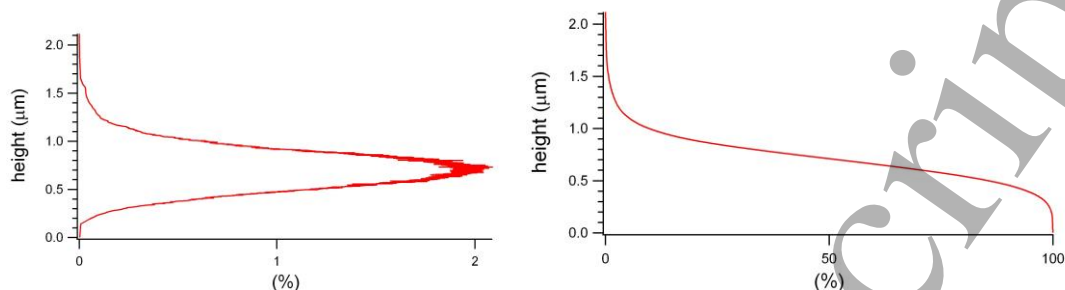
515 Figure 1: Example showing the typical shape of an height distribution (left) and the corresponding Abbott-
516 Firestone curve (right).

517

518 According to the ISO 12178 standard, the three functional parameters studied in this work have been determined
519 by considering the secant to the Abbott-Firestone curve, passing through the points corresponding to the value of
520 of 0% and 40% on the horizontal axis. The procedure consists in traslating these two points along the horizontal
521 axis by maintaining the horizontal relative distance of 40% until the absolute value of the slope of the secant to
522 the curve reaches a minimum [59]. This final situation is represented by the dashed line shown in the scheme in
523 fig. 2.

524
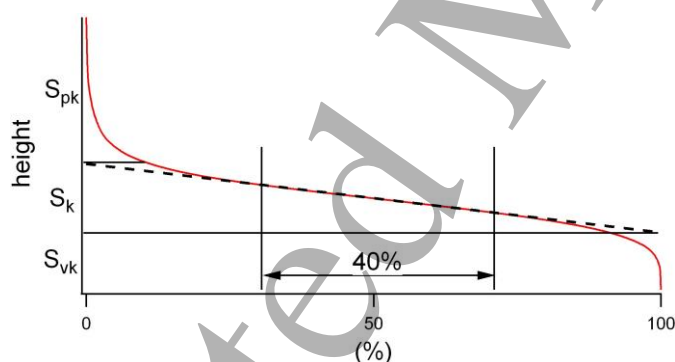
527 Figure 2: Scheme showing the the Abbott-Firestone curve and the corresponding functional parameters *Sk*, *Spk*
528 and *Svk*.

529

530 At this point the functional parameters *Sk*, *Spk* and *Svk* are defined as the lengths shown in fig. 2.

531

537 **References**

538

539 [1] Liu K and Jiang L 2011 Bio-inspired design of multiscale structures for function integration *Nano Today***6**
540 155

541

542 [2] Bhushan B 2016 *Biomimetics: bioinspired hierarchical-structured surfaces for green science and technology*
543 (Berlin: Springer)

544

545 [3] Bhushan B 2009Biomimetics: lessons from nature–an overview*Phil Trans R Soc A***367** 1445

546

547 [4] Aizenberg J and Fratzl P 2009Biological and biomimetic materials*Adv Mater*21 387

548

549 [5] Yao X, Song Y and Jiang L 2011 Applications of Bio-Inspired Special Wettable Surfaces *Adv Mater* 23 387

550

551 [6] Kumar C G and Anand S K 1998 Significance of microbial biofilms in food industry: a review. Int J Food
552 Microbiol**42** 9

553

554

555 [7] Katsikogianni M and Missirlis Y F 2004Concise review of mechanisms of bacterial adhesion to biomaterials
556 and of techniques used in estimating bacteria-material interactions *Eur Cell Mater***8** 37

557

558 [8] Teh K H, Flint S, Brooks J and Knight G 2015 *Biofilms in the Dairy Industry* (Chichester: Wiley)

559

560 [9] Xia F and Jiang L 2008 BBio-inspired, smart, multiscale interfacial materials*Adv Mater.***20** 2842

561

562 [10] Chen F, Zhang D, Yang Q, Yong J, Du G, Si J, Yun F and Hou X 2013 Bioinspired Wetting Surface via
563 Laser Microfabrication *ACS Appl Mater Interfaces* 5 6777

564

565 [11] Bhushan B and Jung Y C 2007Wetting study of patterned surfaces for superhydrophobicity
566 *Ultramicroscopy***107** 1033

567

568 [12] Wu D, Wang J, Wu S, Chen Q, Zhao S, Zhang H, Sun H and Jiang L 2011Three-Level Biomimetic
569 Rice-Leaf Surfaces with Controllable Anisotropic Sliding *Adv Funct Mater***21** 2927

570

571 [13] Ko D, Tumbleston J R, Henderson K J, Euliss L E, DeSimone J M, Lopez R and Samulski E T
572 2011Biomimetic microlens array with antireflective "moth-eye" surface*Soft Matter***7** 6404

573

574 [14] Leem J W, Guan X, Choi M and Yu J S 2015 Broadband and omnidirectional highly-transparent
575 coverglasses coated with biomimetic moth-eye nanopatterned polymer films for solar photovoltaic system
576 applications *Sol Energ Mat Sol C***134** 45

577

578 [15] Lee H, Lee B P and Messersmith P B 2007 A reversible wet/dry adhesive inspired by mussels and geckos
579 *Nature***448** 338

580

581 [16] Feng J, Tuominen M T and Rothstein J P 2011 Hierarchical Superhydrophobic Surfaces Fabricated by
582 Dual-Scale Electron-Beam-Lithography with Well-Ordered Secondary Nanostructures*Adv Funct Mater***126** 62

583

584 [17] Peng S, Tian D, Yang X and Deng W 2014Highly efficient and large-scale fabrication of superhydrophobic
585 alumina surface with strong stability based on self-congregated alumina nanowires*Appl Mater Interfaces***6** 4831

586

587 [18] Zhang B T, Liu B L, Deng X B, Cao S S, Hou X H and Chen H L 2008Fabricating superhydrophobic
588 surfaces by molecular accumulation of polysiloxane on the wool textile finishing*Colloid Polym Sci***286** 453

589

[19] Lu X Y, Zhang J L, Zhang C C and Han Y C 2005 Low-Density Polyethylene (LDPE) Surface With a Wettability Gradient by Tuning its Microstructures *Macromol Rapid Comm* **26** 637

[20] Giljean S, Bigerelle M, Anselme K and Haidara H 2011 New insights on contact angle/roughness dependence on high surface energy materials *Appl Surf Sci* **257** 9631

[21] Manca M, Cannavale A, De Marco L, Arico A S, Cingolani R and Gigli G 2009 Durable superhydrophobic and antireflective surfaces by trimethylsilanized silica nanoparticles-based sol− gel processing *Langmuir* **25** 6357

[22] Taurino R, Fabbri E, Messori M, Pilati F, Pospiech D and Synytska A 2008 Facile preparation of superhydrophobic coatings by sol–gel processes *J Coll Interf Sci* **325**, 149

[23] Fadeeva E, Truong V K, Stiesch M, Chichkov B N, Crawford R J, Wang J and Ivanova E P Bacterial retention on superhydrophobic titanium surfaces fabricated by femtosecond laser ablation *Langmuir* **27** 3012

[24] Truong V K, Webb H K, Fadeeva E, Chichkov B N, Wu A H F, Lamb R, Wang J Y, Crawford R J and Ivanova E P 2012 Air-directed attachment of coccoid bacteria to the surface of superhydrophobic lotus-like titanium *Biofouling* 28 539

[25] Ahmmed K M T, Grambow C and Kietzig A 2014 Fabrication of micro/nano structures on metals by femtosecond laser micromachining *Micromachines* **5** 1219

[26] Jiang X, Scott P J, Whitehouse D J and Blunt L 2007 Paradigm shifts in surface metrology. Part II. The current shift *P Roy Soc A-Math Phy* **463** 2071

[27] Leach R 2013 Introduction to surface topography. In *Characterisation of Areal Surface Texture* (Berlin: Springer)

[28] Suh A Y, Polycarpou A A and Conry T F Detailed surface roughness characterization of engineering surfaces undergoing tribological testing leading to scuffing *Wear* **255** 556

[29] Goodhand M N, Walton K, Blunt L, Lung H W, Miller R J and Marsden R 2016 The limitations of using R_a to describe surface roughness The Limitations of Using "Ra" to Describe Surface Roughness *J Turbomach* **138** 101003

[30] Jullien C, Bénézech T, Carpentier B, Lebret V and Faille C 2003 Identification of surface characteristics relevant to the hygienic status of stainless steel for the food industry *J Food Eng* **56** 77

[31] Faille C, Membre J M, Ussier J P, Bellon-Fontaine M N, Carpentier B, Laroche M A and Benezech T 2000 Influence of physicochemical properties on the hygienic status of stainless steel with various finishes *Biofouling* **15**, 261

[32] Leclercq-Perlat M N and Lalande M 1994 Cleanability in relation to surface chemical composition and surface finishing of some materials commonly used in food industries *J FoodEng* **23** 501

[33] Wirtanen G, Ahola H and Mattila-Sandholm T 1996 Evaluation of cleaning procedures for elimination of biofilm from stainless steel surfaces in open process equipment *EUR* 167

[34] Barnes L M, Lo M F, Adams M R and Chamberlain A H L 1999 Effect of milk proteins on adhesion of bacteria to stainless steel surfaces *Appl Environ Microbiol* **65** 4543

[35] Wang X, Li Y, Onnis-Hayden A, Gao C, Gu A Z and Wan K T 2012 Correlation of macroscopic aggregation behavior and microscopic adhesion properties of bacteria strains using a dimensionless Tabor's parameter *J CollInterfSci* **374** 70

[36] Wang X Li Y, Gu A Z and Wan K T 2013 Predicting macroscopic colloidal deposition and transportation based on dimensionless Tabor's parameter *Nano Life***3** 1340009

[37] Li Y, Wang X, Onnis-Hayden A, Wan K T and Gu A Z 2014 Universal Quantifier Derived from AFM Analysis Links Cellular Mechanical Properties and Cell–Surface Integration Forces with Microbial Deposition and Transport Behavior *Environ SciTechnol***48** 1769

[35] Crawford R J, Webb H K, Truong V K, Hasan J and Ivanova E P 2012 Surface topographical factors influencing bacterial attachment *Adv Coll Interfac***179** 142

[36] Scheuerman T R, Camper A K and Hamilton M A 1998 Effects of substratum topography on bacterial adhesion *J Coll Interf Sci***208** 23

[37] Verran J and Maryan C J 1997Retention of Candida albicans on acrylic resin and silicone of different surface topography*J Prosthet Dent***77** 535

[38] Whitehead K A, Colligon J and Verran J 2005 Retention of microbial cells in substratum surface features of micrometer and sub-micrometer dimensions *Colloid Surface B***41** 129

[39] Ivanova E P, Truong V K, Webb H K, Baulin V A, Wang J Y, Mohammodi N, Wang F, Fluke C and Crawford R J 2011 Differential attraction and repulsion of Staphylococcus aureus and Pseudomonas aeruginosa on molecularly smooth titanium films *Sci Rep***1** 165

[40] Verran J, Packer A, Kelly P and Whitehead K A 2010 The retention of bacteria on hygienic surfaces presenting scratches of microbial dimensions *Lett Appl Microbiol***50** 258

[41] Lorenzetti M, Dogša I, Stošvicki T, Stopar D, Kalin M, Kobe S and Novak S 2015The influence of surface modification on bacterial adhesion to titanium-based substrates*ACS Appl Mater Interfaces***7** 1644

[42] Bollen C M, Lambrechts P and Quirynen M 1997 Comparison of surface roughness of oral hard materials to the threshold surface roughness for bacterial plaque retention: a review of the literature*Dent Mater***13** 258

[43] Scardino A J, Harvey E and De Nys R 2006 Testing attachment point theory: diatom attachment on microtextured polyimide biomimics *Biofouling***22** 55

[44] Mincuzzi G, Gemini L, Faucon M and Kling R 2016 Extending ultra-short pulse laser texturing over large area *Appl Surf Sci***386** 65

[45] Gemini L, Hashida M, Shimizu M, Miyazaka Y, Inoue S, Tokita S, Limpouch J,Mocek T and Sakabe S2013Metal-like self-organization of periodic nanostructures on silicon and silicon carbide under femtosecond laser pulses*J Appl Phys***114** 194903

[46] Bonse J, Krüger J, Höhm S and Rosenfeld A 2012 Femtosecond laser-induced periodic surface structures *J Laser Appl***24** 042006

[47] Bonse J, Hohm S, Kirner S V, Rosenfeld A and Kruger J 2017 Laser-Induced Periodic Surface Structures— A Scientific Evergreen*IEEE J Sel Top Quan Electr***23** 9000615

[48] Tsibidis G D, Fotakis C andStratakis E 2015From ripples to spikes: A hydrodynamical mechanism to interpret femtosecond laser-induced self-assembled structures*Phys Rev B***92** 041405

[49] Gadelmawla E S, Koura M M, Maksoud T M A, Elewa I M andSoliman H H 2002Roughness parameters*J Mater Process Tech***123** 133

[50] Neuenschwander B, Jaeggi B, Schmid M, Rouffiange V and Martin P E2012 Optimization of the volume ablation rate for metals at different laser pulse-durations from ps to fs In *SPIE LASE* 824307

[51] Kietzig A M, Hatzikiriakos S G andEnglezos P 2009 Patterned superhydrophobic metallic surfaces.*Langmuir***25**, 4821

[52] Kathiresan S and Mohan B 2017 In-vitro bacterial adhesion study on stainless steel 316L subjected to magneto rheological abrasive flow finishing *Biomed Res* **28**, 7

[53] Rochford E T J, Poulsson A H C, Varela J S, Lezuo P, Richards R G and Moriarty T F 2014 Bacterial adhesion to orthopaedic implant materials and a novel oxygen plasma modified PEEK surface *Colloids Surface B* **113**, 213

[54] Zhao Q, Liu Y, Wang C, Wang S, Peng N and Jeynes C 2008 Reduction of bacterial adhesion on ion-implanted stainless steel surfaces. Medical engineering & physics **30**, 341

[55] Shaikh S, Singh D, Subramanian M, Kedia S, Singh A K, Singh K, Gupta N and Sinha S 2017 Femtosecond laser induced surface modification for prevention of bacterial adhesion on 45S5 bioactive glass *arXiv preprint* arXiv:1706.06327

[56] Crawford R J, Webb H K, Truong V K, Hasan J and Ivanova E P 2012 Surface topographical factors influencing bacterial attachment *Adv colloid interf* **179**, 142

[57] Thomas T R 1999 *Rough surfaces* (London:Imperial College Press)

[58] Leach R 2013 *Characterisation of areal surface texture* (Heidelberg:Springer)

[59] Blunt L and Jiang X 2003 *Advanced techniques for assessment surface topography: development of a basis for 3D surface texture standards "surfstand"* (Elsevier)